Side-Chain Liquid Crystalline Poly(meth)acrylates with Bent-Core Mesogens

Xiaofang Chen,[†,‡] Kishore K. Tenneti,[‡] Christopher Y. Li,[*,‡] Yaowen Bai,[†] Xinhua Wan,[†] Xinghe Fan,[†] Qi-Feng Zhou,[*,†] Lixia Rong,[§] and Benjamin S. Hsiao[§]

Department of Polymer Science and Engineering and The Key Laboratory of Polymer Chemistry and Physics of Ministry of Education, College of Chemistry, Peking University, Beijing 100871, P. R. China; A.J. Drexel Nanotechnology Institute and Department of Materials Science and Engineering, Drexel University, Philadelphia Pennsylvania 19104; and Department of Chemistry, Stony Brook University, Stony Brook, New York 11794

Received August 23, 2006; Revised Manuscript Received December 2, 2006

ABSTRACT: We report the design, synthesis, and characterization of side-chain liquid crystalline (LC) poly(meth)acrylates with end-on bent-core liquid crystalline (BCLC) mesogens. Both conventional free radical polymerization and atom transfer radical polymerization have been used to synthesize these liquid crystalline polymers (LCP). The resulting polymers exhibit thermotropic LC behavior. Differential scanning calorimetry, thermopolarized light microscopy, wide-angle X-ray diffraction, and small-angle X-ray scattering were used to characterize the LC structure of both monomers and polymers. The electro-optic (EO) measurement was carried out by applying a triangular wave and measuring the LC EO response. SmCP (Smectic C indicates the LC molecules are tilted with respect to the layer normal; P denotes polar ordering) phases were observed for both monomers and polymers. In LC monomers, typical antiferroelectric switching was observed. In the ground state, $SmCP_A$ (A denotes antiferroelectric) was observed which switched to $SmCP_F$ (F denotes ferroelectric) upon applying an electric field. In the corresponding LCP, a unique bilayer structure was observed, which is different from the reported BCLC bilayer SmCG (G denotes generated) phase. Most of the LCPs did not switch upon applying electric field while weak AF switching was observed in a low molecular weight poly{(3′-[4-(4-*n*-dodecyloxybenzoyloxy)benzoyloxy]-4-(12-acryloyloxydodecyloxy)benzoyloxybiphenyl} sample.

Introduction

Because of their fascinating structure and profound electro-optic (EO) applications, chiral liquid crystals (LC) have been of great interest during the past century.[1] Most of the chiral LCs are induced by the asymmetric chemical groups, while recently symmetry breaking in LC was achieved by introducing achiral bent-core liquid crystalline (BCLC) mesogens.[2] Because of the unique mesogen shape, BCLCs are also known as banana LCs. Extensive research has been devoted to reveal the nature of the chirality, structure formation, and EO properties of BCLCs.[3−10] Symmetry breaking is attributed to tilting of the bent mesogen, as shown in Scheme 1. Three directions can be defined for a particular smectic BCLC structure: the molecular axis **n**, the polarization axis **P**, and the molecular plane normal **m** which is perpendicular to both **n** and **P**. In addition, molecular tilting direction (**c**) in SmCP (Smectic C indicates the LC molecules are tilted with respect to the layer normal; P denotes polar ordering) phase is of crucial importance in determining BCLC chirality. On the basis of **P**, **c**, and the smectic layer normal direction, both (+) and (−) chirality can be defined as shown in Scheme 1. Unique ferroelectric (F) and antiferroelectric (AF) behaviors have been observed. The banana phases were first identified as B1−B7 (B stands for banana, bent, bow, or boomerang). As their structures were gradually understood, SmCP as well as columnar phase (Col) was used to interpret different banana phases. In particular, the B2 phase was defined as $SmCP_A$ (A stands for antiferroelectric), which can be switched to SmC_SP_F (S denotes synclinic) or SmC_AP_F (A denotes anticlinic) under an external electric field. The most complex BCLC structure, the B7 phase, was recently explained using either modulated/undulated layered SmCP or SmCPG (G denotes generated) model.[5] Bilayer SmCP phases have also been reported.[11−15]

Although BCLCs have been extensively investigated, research on BCLC polymers is still limited. A few polymerizable BCLC

Scheme 1. Schematic Representation of Bent-Core Liquid Crystalline Mesogens and Their Different Chiral States[a]

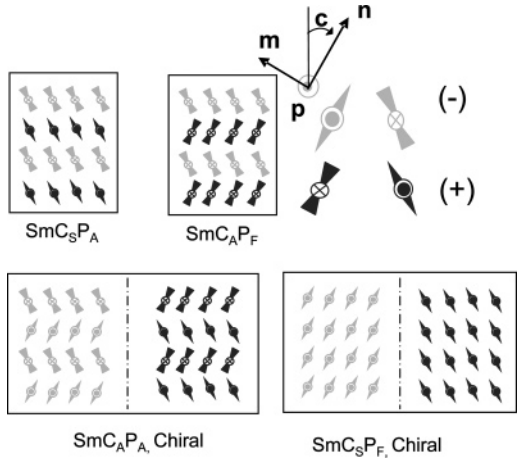

[a] SmCP: smectic C indicates the LC molecules are tilted with respect to the layer normal; P denotes the smectic layers are polar. $SmCP_A$ (A stands for antiferroelectric) and $SmCP_F$ (F stands for ferroelectric) can be switched to SmC_SP_F (S denotes synclinic) or SmC_AP_F (A denotes anticlinic).

* Corresponding authors. Christopher Li: Ph 215-895-2083; Fax 215-895-6760; e-mail chrisli@drexel.edu. Qi-Feng Zhou: Ph 86-10-62756660; e-mail qfzhou@pku.edu.cn.

† Peking University.

‡ Drexel University.

§ Stony Brook University.

10.1021/ma061949u CCC: $37.00
Published on Web 01/26/2007

Scheme 2. Chemical Structures of Side-Chain Poly(meth)acrylates with Bent-Core Mesogens

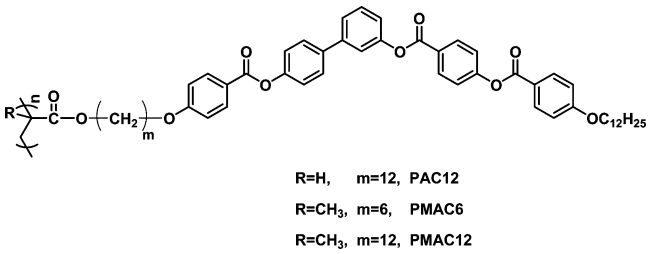

systems have been reported.[16−29] In most of these cases, polymerizable groups, such as 1,3-diene,[19] di(meth)acrylates,[21] or vinyl group,[17,20,22−24] were symmetrically attached in both ends, some of which could be thermally or optically cross-linked to form BCLC networks.[16,19,21] Polarized polymeric materials with pyroelectric properties could be achieved when those monomers were polymerized in the B2 phase under the external electric field.[19] Nematic phase was found when ester-type banana mesogens were introduced in polymer main chain together with rodlike mesogens synthesized via alternating diene metathesis polycondensation.[22,30] Furthermore, B1 and B2 phases could be formed in main-chain polymers with azomethine-type mesogens, but the high viscosity and high phase transition temperature restricted further investigation.[31] BCLC mesogens have also been used to side attach to the polymer backbone, leading to a unique type of bent-core mesogen jacketed LC polymers.[32] Recently, the first BCLC side-chain, end-attached LC polymer with polysiloxane as the backbone was reported. Hydrosilylation reaction was used to couple the BCLC mesogens onto the polysiloxane backbone, and the density of the mesogens was relatively low to ensure the switching behavior (the ratio of BCLC mesogen and the siloxane repeating unit was ∼1:15).[33] Block copolymer-like, phase-separated structure was proposed, and F switching behavior was also observed.

In this article, we report the design, synthesis, and characterization of the first side-chain BCLC polymers with poly(meth)acrylate backbone (Scheme 2). Instead of hydrosilylation reaction, direct polymerization of BCLC monomers via conventional free radical polymerization (FRP) or atom transfer radical polymerization (ATRP) was conducted, granting the high BCLC mesogen density in the resulting LCP. EO switching behaviors were investigated. All of the side-chain BCLC polymers showed bilayer SmCP structure, which is, to the best of our knowledge, the first time that this structure was observed in BCLC polymers. Detailed structure analysis and formation mechanism will be discussed.

Experimental Section

Materials. 4-(Dimethylamino)pyridine (DMAP, 99%), triphenylphosphine (99%), 3-bromophenol (99%), ethyl 2-bromopropionate (EBP, 99%), and trimethyl borate (99%) were used as received from Acros. *p*-Hydroxybenzoic acid (99%), 1-bromododecane (98%), *N*,*N*′-dicyclohexylcarbodiimide (DCC, 95%), 4-bromophenol (99%), benzyl bromide (99%), diethyl azodicarboxylate (DEAD, 99%), ethyl *p*-hydroxybenzoate (99%), palladium carbon catalyzer, and *p*-toluenesulfonic acid (99%) were used as received from Beijing Chemical Co. Benzyl 4-hydroxybenzoate (99%) was used as received from Aldrich. 1,12-Dodecanediol (98%) and 1,6-hexanediol (98%) were used as received from Fluka. *N*,*N*,*N*′,*N*′,*N*″-Pentamethyldiethylenetriamine (PMDETA, 98%) was used as received from TCI. Azobis(isobutyronitrile) (AIBN) was recrystallized before use. Cuprous bromide (CuBr) was synthesized from $CuBr_2$ and purified by stirring in acetic acid and washing with methanol followed by drying in vacuum before use. Tetrahydrofuran (THF) and benzene were refluxed over sodium under argon and distilled out before use. Chlorobenzene was refluxed over CaH_2 and distilled before use.

Scheme 3. Synthesis of Bent-Core Liquid Crystalline Monomers, 3′-[4-(4-*n*-Dodecyloxybenzoyloxy)benzoyloxy]-4-(12′-acryloyloxydodecyloxy)benzoyloxybiphenyl (AC12), 3′-[4-(4-*n*-Dodecyloxybenzoyloxy)benzoyloxy]-4-(6′-methacryloyloxyhexyloxy)benzoyloxybiphenyl (MAC6), and 3′-[4-(4-*n*-Dodecyloxybenzoyloxy)benzoyloxy]-4-(12′-methacryloyloxydodecyloxy)benzoyloxybiphenyl (MAC12)[a]

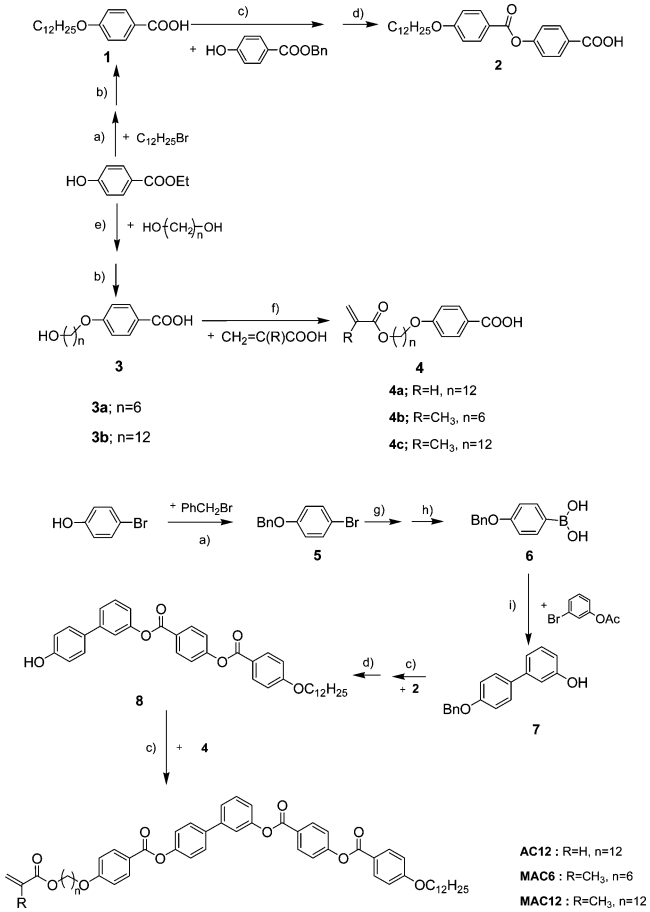

[a] (a) K_2CO_3, acetone, reflux; (b) KOH, ethanol, reflux; (c) *N*,*N*′-dicyclohexylcarbodiimide, 4-(dimethylamino)pyridine, dichloromethane, rt; (d) H_2, 5% Pd−C, 1,4-dioxane, rt; (e) diethyl azodicarboxylate, PPh_3, tetrahydrofuran (THF), reflux; (f) *p*-sulfonbenzene acid, chloroform, reflux; (g) Mg, THF, reflux; (h) trimethyl borate, THF, −78 °C; (i) $Pd(PPh_3)_4$, $NaHCO_3$, H_2O, glyme, reflux.

Synthesis of Monomers. The synthetic route to obtain the monomer is depicted in Scheme 3. These compounds were prepared according to the synthetic routes similar to those reported in the literature with minor modifications.[21,34,35] Detailed synthesis of intermediates and precursors is presented in the Supporting Information.

3′-[4-(4-*n*-Dodecyloxybenzoyloxy)benzoyloxy]-4-(12-acryloyloxydodecyloxy)benzoyloxybiphenyl (AC12). 8 (5.95 g, 10.0 mmol), **4a** (3.77 g, 10.0 mmol), DCC (2.06 g, 10.0 mmol), and DMAP (0.12 g, 1 mmol) were dissolved in dichloromethane. The solution was stirred at room temperature for about 8 h. The precipitate was filtered and washed with dichloromethane several times. After evaporation of the solvent, the obtained ester was purified by silica gel column chromatography with dichloromethane as the eluent to yield 5.72 g (60%) of AC12 as a white solid. ^{1}H NMR (δ, ppm): 0.88−0.90 (t, 3H, $-CH_3$), 1.27−1.85 (m, 44H, $-CH_2-$), 4.04−4.07 (m, 4H, $-OCH_2-$), 4.13−4.17 (t, 2H, $-OCH_2-$), 5.80−6.38 (t, 3H, $CH_2{=}CH-$), 6.90−8.32 (m, 20H, Ar−H). ^{13}C NMR (δ, ppm): 14.09 ($-CH_2CH_3$), 22.65−31.88

(−(CH_2)$_{10}$$CH_3$), 64.66 ($CH_2$=CHCOO$CH_2$), 68.28−68.35 ($CH_2$-OAr), 114.27−114.38 (aromatic C *ortho* to OCH_2), 120.38−120.52 (aromatic *C ortho* to OC=O), 120.91−121.42 (aromatic *C* to C=O), 122.08−122.15 (aromatic *C ortho* to OC=O), 124.64 (center phenyl *C para* to O), 126.82 (aromatic C to C=O), 128.20 (aromatic *C ortho* to center phenyl ring), 128.61 (CH_2=*C*HCOOCH$_2$), 129.81 (aromatic *C* meta to O), 130.37 (*C*H_2=CHCOOCH$_2$), 131.79−132.38 (aromatic C *ortho* to C=O), 137.71−155.39 (aromatic *C*−O−C=O), 163.55−163.79 (aromatic *C*−OCH_2), 164.27−164.43 (*C*=O), 164.87 (CH_2=CH−*C*=O). Anal. Calcd for $C_{60}H_{72}O_{10}$ (M = 953.21): C, 75.60; H, 7.61. Found: C, 75. 58; H, 7.63.

3′-[4-(4-*n*-Dodecyloxybenzoyloxy)benzoyloxy]-4-(6-methacryloyloxyhexyloxy)benzoyloxybiphenyl (MAC6). Esterification of **8** (5.95 g, 10.0 mmol) and **4b** (3.06 g, 10.0 mmol) was carried out following the same procedure as above, to yield 5.73 g (65%) of MAC6 as a white powder. ^{1}H NMR (δ, ppm): 0.88−0.90 (t, 3H, −C*H*$_3$), 1.29−1.73 (m, 28H, −C*H*$_2$−), 1.94 (t, 3H, CH_2=C(C*H*$_3$)−), 4.01−4.06 (q, 4H, −OC*H*$_2$−), 4.12−4.14 (t, 2H, −OC*H*$_2$−), 5.54 (s, 1H, C*H*$_2$=C(CH$_3$)−), 6.10 (s, 1H, C*H*$_2$=C(CH$_3$)−), 6.94−8.31 (q, 20H, Ar−*H*). ^{13}C NMR (δ, ppm): 14.11 (−CH_2*C*H$_3$), 18.33 (−CH_2=C(*C*H$_3$)−), 22.66−33.5 (−*C*H$_2$−), 64.56 (CH_2=C(CH$_3$)-COO*C*H$_2$), 68.03−68.33 (*C*H$_2$OAr), 113.94−114.35 (aromatic C *ortho* to OCH_2), 120.38−120.53 (aromatic *C ortho* to OC=O), 120.84−121.44 (aromatic *C* to C=O), 121.90−122.11 (aromatic *C ortho* to OC=O), 124.66 (center phenyl *C para* to O), 125.03 (*C*H_2=C(CH$_3$)COOCH$_2$), 126.77 (aromatic C to C=O), 128.21 (aromatic *C ortho* to center phenyl ring), 129.83 (aromatic *C* meta to O), 131.80−132.38 (aromatic C ortho to C=O), 136.41 (CH_2=*C*(CH$_3$)COOCH$_2$), 137.70−155.36 (aromatic *C*−O−C=O), 163.43−165.88 (*C*=O), 167.49 (CH_2=C(CH$_3$)*C*=O). Anal. Calcd for $C_{55}H_{62}O_{10}$ (M = 883.07): C, 74.81; H, 7.08. Found: C, 74. 89; H, 7.06.

3′-[4-(4-*n*-Dodecyloxybenzoyloxy)benzoyloxy]-4-(12-methacryloyloxydodecyloxy)benzoyloxybiphenyl (MAC12). Esterification of **8** (5.95 g, 10.0 mmol) and **4c** (3.90 g, 10.0 mmol) was carried out following the same procedure as above, to yield 7.16 g (74%) of MAC12 as a white powder. ^{1}H NMR (δ, ppm): 0.87−0.90 (t, 3H, −C*H*$_3$), 1.27−1.83 (m, 40H, −C*H*$_2$−), 1.94 (t, 3H, CH_2=C(C*H*$_3$)−), 4.01−4.06 (q, 4H, −OC*H*$_2$−), 4.12−4.15 (t, 2H, −OC*H*$_2$−), 5.54 (s, 1H, C*H*$_2$=C(CH$_3$)−), 6.10 (s, 1H, C*H*$_2$=C(CH$_3$)−), 6.96−8.30 (q, 20H, Ar−*H*). ^{13}C NMR (δ, ppm): 14.06 (−CH_2*C*H$_3$), 18.25 (−CH_2=C(*C*H$_3$)−), 22.62−31.85 (−*C*H$_2$−), 64.73 (CH_2=C(CH$_3$)COO*C*H$_2$), 68.24−68.30 (*C*H$_2$OAr), 114.24−114.35 (aromatic C *ortho* to OCH_2), 120.33−120.48 (aromatic *C ortho* to OC=O), 120.88−121.39 (aromatic *C* to C=O), 122.04−122.11 (aromatic *C ortho* to OC=O), 124.57 (center phenyl *C para* to O), 125.03 (*C*H_2=C(CH$_3$)COOCH$_2$),126.77 (aromatic C to C=O), 128.14 (aromatic *C ortho* to center phenyl ring), 129.76 (aromatic C meta to O), 131.74−132.34 (aromatic C ortho to C=O), 136.49 (CH_2=*C*(CH$_3$)COOCH$_2$), 137.64−155.36 (aromatic *C*−O−C=O), 163.51−164.36 (*C*=O), 167.43 (CH_2=C(CH$_3$)*C*=O). Anal. Calcd for $C_{61}H_{74}O_{10}$ (M = 967.23): C, 75.75; H, 7.71. Found: C, 75. 77; H, 7.69.

Polymerization. Free Radical Polymerization (FRP). A typical polymerization procedure is summarized as the following. MAC12 (0.40 g, 0.41 mmol), 27 μL of 0.05 M AIBN solution in benzene, and benzene (2 mL) were transferred into a polymerization tube. After three freeze−pump−thaw cycles, the tube was sealed off under vacuum. Polymerization was carried out at 60 °C for 24 h. The tube was then opened, and the reaction mixture was diluted with 10 mL of CH_2Cl_2. After evaporation of the solvent, the products were purified through column chromatography with CH_2Cl_2 as the eluent in order to remove unreacted monomers. Polymer was obtained by precipitation in methanol followed by drying under vacuum at room temperature for 24 h to yield 0.3 g (72%) as a white powder; $GPC_{PSt,THF}$, M_n (number-average molecular weight) = 2.2 × 10^5, polydispersity index (PDI) = M_w (weight-average molecular weight)/M_n = 1.4. The removal of the monomer from the polymer was confirmed by ^{1}H NMR spectra and GPC results.

Atom Transfer Rradical Polymerization (ATRP). A typical procedure is summarized as the following: MAC12 (0.39 g, 0.40 mmol), CuBr (1.5 mg, 0.01 mmol), PMDETA (1.8 mg, 0.010 mmol), EBP (1.8 mg, 0.010 mmol), and chlorobenzene (2 mL) were added into a 10 mL reaction tube. The reaction mixture was purged with nitrogen and subjected to three freeze−thaw cycles and then sealed under vacuum. Polymerization was carried out at 60 °C for 12 h. The tube was then opened, and the reaction mixture was diluted with THF. Then the solution was passed through a basic aluminum oxide column to remove the copper complex. After evaporation of the solvent, the products were purified through column chromatography with CH_2Cl_2 as the eluent in order to remove unreacted monomers. Polymer was obtained by precipitation in methanol followed by drying under vacuum at room temperature for 24 h, to yield 0.30 g (77%) as a white powder; $GPC_{PSt,THF}$, M_n = 4.0 × 10^4, PDI = M_w/M_n = 1.4. The removal of the monomer from the polymer was confirmed by ^{1}H NMR spectra and GPC results.

Scheme 4. Schematic Representation of the Shear Geometry

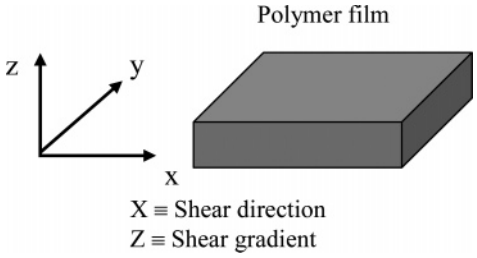

Equipment and Sample Preparation. ^{1}H NMR (400 MHz) spectra and ^{13}C NMR (100 MHz) were recorded on a Bruker ARX400 spectrometer using $CDCl_3$ as solvent; the chemical shifts referred to the internal tetramethylsilane peak. Elemental analyses were recorded on an Elementar Vario EL instrument. Gel permeation chromatographic (GPC) measurements were performed with a Waters 515 HPLC pump and a 2410 refractive index detector at 35 °C, and THF was used as the eluent at a flow rate of 1.0 mL/min. Three Waters Styragel columns with 10 μm bead size were connected in series. Their effective molecular weight ranges were 100−10 000 g/mol for Styragel HT2, 500−30 000 g/mol for Styragel HT3, and 5000−600 000 g/mol for Styragel HT4. The pore sizes are 50, 100, and 1000 nm for Styragel HT2, HT3, and HT4, respectively. All GPC data were calibrated with polystyrene standards. The samples were dissolved in THF (10 mg/mL) and filtered through a 0.45 μm PTFE filter before the measurements.

The thermal transitions of the monomers and polymers were detected using a Perkin-Elmer DSC-7 differential scanning calorimeter. The temperature and heat flow were calibrated using standard materials (indium and zinc) at different cooling and heating rates between 5 and 40 °C/min. Samples with a typical mass of 2−4 mg were encapsulated in sealed aluminum pans. A controlled cooling experiment was always carried out first, and a subsequent heating was performed at a rate that was equal to or faster than the previous cooling. The inflection point temperature was used to determine the glass transition temperature, and peak (endothermic maximum) temperature was used to determine the isotropization temperature of the LCs. Thermogravimetric analyses (TGA) were performed on a TA SDT 2960 instrument.

Phase morphology and LC defects were observed using polarized light microscopy (PLM, Olympus BX-51) coupled with a Mettler hot stage (FP 82 HT with a FP-90 central processor). The image was captured using an Insight digital camera.

Two-dimensional (2-D) wide-angle X-ray diffraction (WAXD) and small-angle X-ray scattering (SAXS) experiments were carried out using synchrotron X-ray beamline X-27C at the National Synchrotron Light Source in Brookhaven National Laboratory. The wavelength of the X-ray beam was 0.1371 nm. The air scattering was subtracted from the WAXD patterns. To achieve orientated diffraction patterns, the samples were sheared, and Scheme 4 shows the shear geometry.

EO properties were studied using 5 μm commercial cells (from Instec Inc.) with parallel rubbed polyimide layers. Switching current

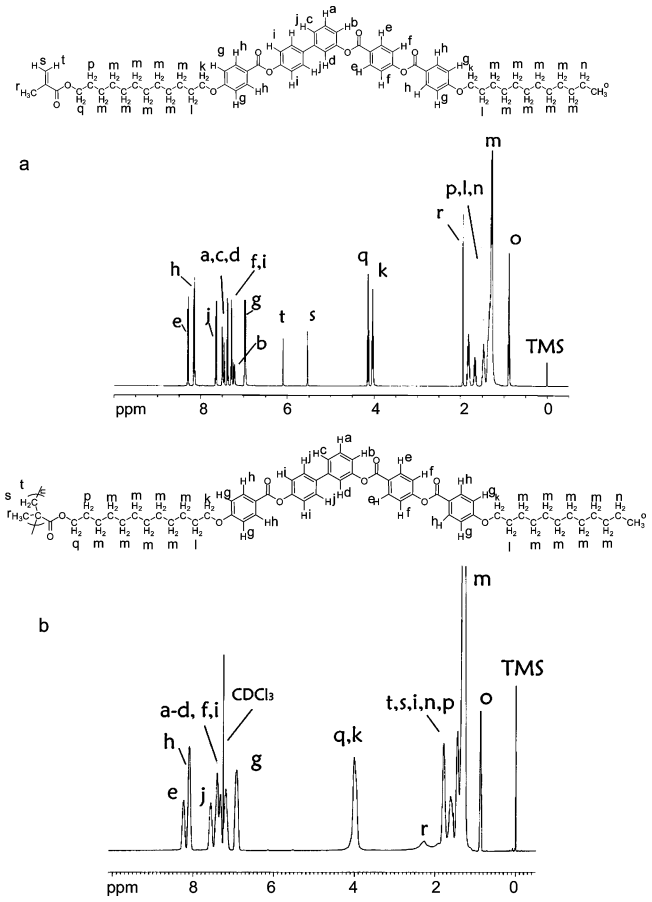

Figure 1. ^{1}H NMR spectra of 3′-[4-(4-*n*-dodecyloxybenzoyloxy)-benzoyloxy]-4-(12-methacryloyloxydodecyloxy)benzoyloxybiphenyl (MAC12) (a) and corresponding polymer poly{3′-[4-(4-*n*-dodecyloxy-benzoyloxy)benzoyloxy]-4-(12-methacryloyloxydodecyloxy)ben-zoyloxybiphenyl} PMAC12 (b).

was measured by applying triangular voltage wave using Instec automatic LC tester (ALCT) equipment. In all the above-mentioned monomer characterization processes, low temperature and/or short time were used in order to avoid monomer polymerization during the sample measurements.

Results and Discussion

Synthesis and Smectic CP Phase of MAC and AC Monomers. Since most of bent-core molecules contain symmetric chemical structures, symmetrically modifying the mesogens with polymerizable groups has been first attempted in the literature. However, asymmetric BCLCs have attracted great attention recently because they may exhibit new phase behavior.[36−40] For asymmetric bent-core mesogen synthesis, the most considered strategy is tuning the feed ratio of the two reactants of esterification to achieve monosubstituted products. In this case, the disubstituted product is regarded as the byproduct which is unavoidable. To address this issue, biphenyl type BCLC mesogen was first designed and reported by Tschierske et al.[41,42] By selective cleavage of protected groups at different chemical conditions, asymmetric BCLC monomer with relatively high yield can be readily achieved.[34] Furthermore, such BCLC mesogens are tolerant of end-group modification: the silicon-containing dimers, dendrimers, and polymers were designed and synthesized successfully without diminishing LC properties of such mesogens. We thus adopted this type of mesogen to thoroughly investigate the phase behavior of side chain BCLC polymers. Chemical structures of these monomers were confirmed with NMR (^{1}H, ^{13}C, and DEPT) and elemental

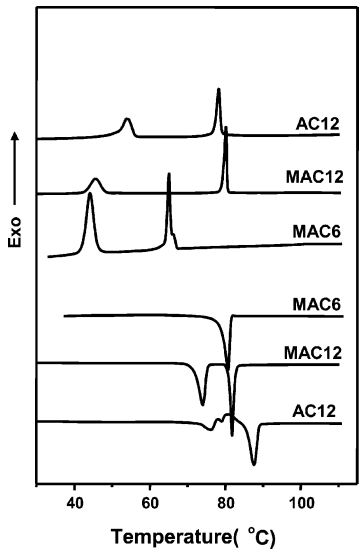

Figure 2. Differential scanning calorimetery thermograms of 3′-[4-(4-*n*-dodecyloxybenzoyloxy)benzoyloxy]-4-(12-acryloyloxydodecyloxy-)benzoyloxybiphenyl (AC12), 3′-[4-(4-*n*-dodecyloxybenzoyloxy)-benzoyloxy]-4-(6-methacryloyloxyhexyloxy)benzoyloxybiphenyl (MAC6), and 3′-[4-(4-*n*-dodecyloxybenzoyloxy)benzoyloxy]-4-(12-methacryloy-loxydodecyloxy)benzoyloxybiphenyl (MAC12) at heating and cooling rate of 10 °C/min.

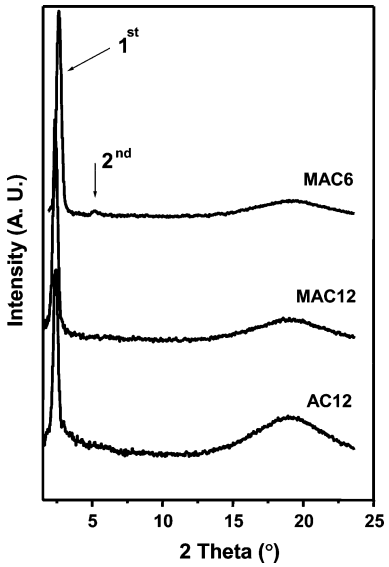

Figure 3. Wide-angle X-ray diffraction profile of 3′-[4-(4-*n*-dodecy-loxybenzoyloxy)benzoyloxy]-4-(12-acryloyloxydodecyloxy)benzoy-loxybiphenyl (AC12) at 75 °C, 3′-[4-(4-*n*-dodecyloxybenzoyloxy)-benzoyloxy]-4-(6-methacryloyloxyhexyloxy)benzoyloxybiphenyl (MAC6) at 62 °C, and 3′-[4-(4-*n*-dodecyloxybenzoyloxy)benzoyloxy]-4-(12-methacryloyloxydodecyloxy)benzoyloxybiphenyl (MAC12) at 75 °C.

analysis. Figure 1a shows the ^{1}H NMR spectra of monomer MAC12. The characteristic resonance of the vinyl group at 6.09 and 5.53 ppm (denoted as t, s in the figure) can be clearly seen.

Figure 2 shows the DSC thermograms of MAC6, MAC12, and AC12. Two transition peaks can be found during cooling and heating in MAC12 and AC12. (For AC12, recrystallization also occurs during heating at ∼80 °C.) The higher temperature transition (T2) possesses the same onset temperature in heating and cooling curves while the lower temperature transition (T1) shows a melting hystersis, indicating that T1 is due to a crystal formation/melting while T2 is due to a LC phase transition. In MAC6, only one transition peak was observed during heating while two peaks were seen in the cooling curve, suggesting a monotropic behavior of MAC6. LC phase structure of these

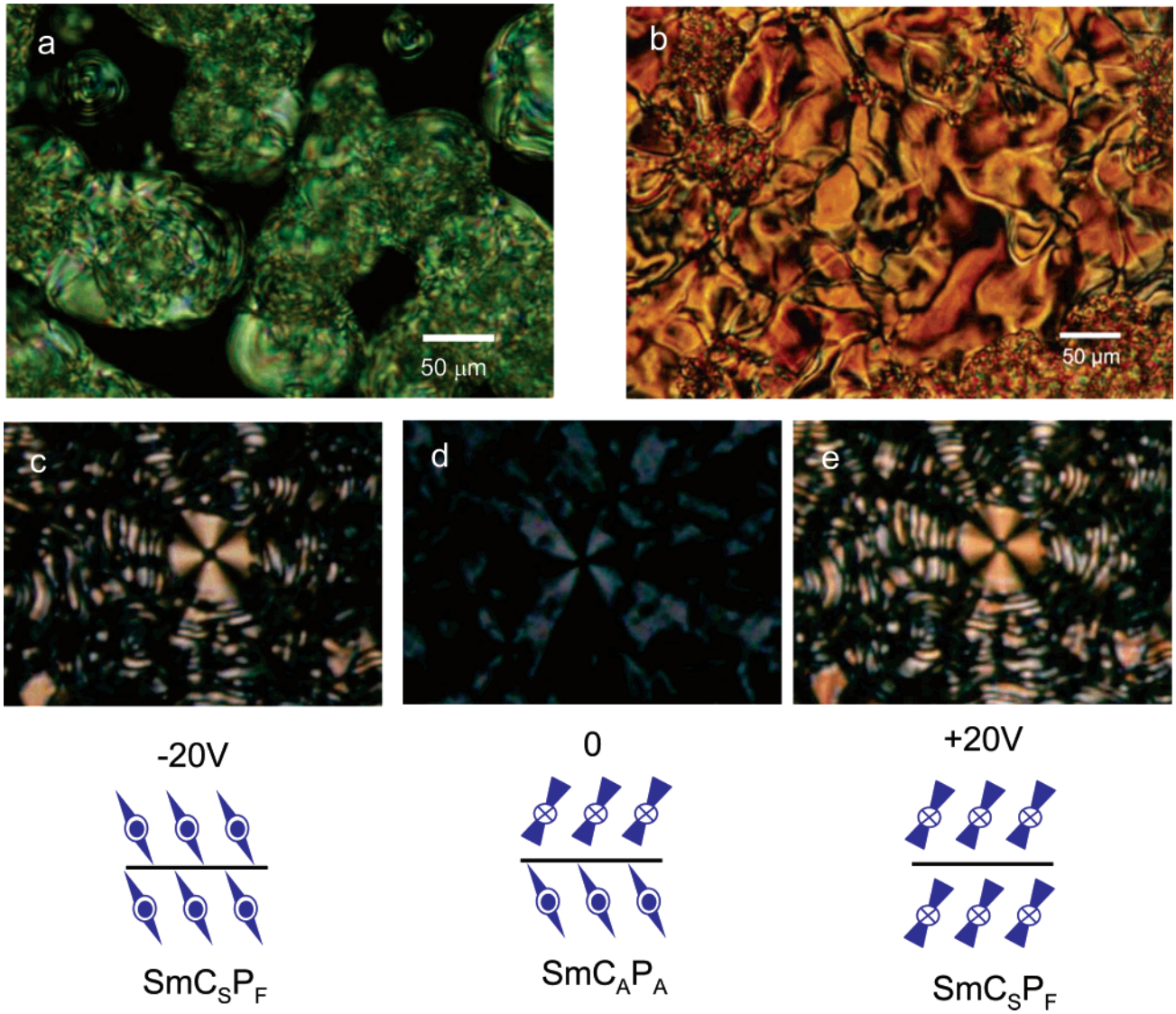

Figure 4. Texture of 3′-[4-(4-*n*-dodecyloxybenzoyloxy)benzoyloxy]-4-(12-acryloyloxydodecyloxy)benzoyloxybiphenyl (AC12) at 70 °C (a) and 3′-[4-(4-*n*-dodecyloxybenzoyloxy)benzoyloxy]-4-(6-methacryloyloxyhexyloxy)benzoyloxybiphenyl (MAC6) at 76 °C (b). The liquid crystal cells were not subjected to an electric field. (c), (d), and (e) show 3′-[4-(4-*n*-dodecyloxybenzoyloxy)benzoyloxy]-4-(12-methacryloyloxydodecyloxy)-benzoyloxybiphenyl (MAC12) at 80 °C under different electric fields. The domains formed after cooling the clear isotropic phase: (c) electric potential, $E = -20$ V, (d) $E = 0$ V, (e) $E = +20$ V. Schematic representations of the corresponding liquid crystalline phases are also shown.

monomers can be confirmed by WAXD experiment, as shown in Figure 3. Several diffraction peaks can be observed in the low-angle region, while in the wide-angle region only amorphous scattering can be observed. The scattering vectors of the low-angle diffractions obey the ratios of 1:2 (see arrows), suggesting a smectic structure. The *d*-spacings of the first-order peaks can be calculated to be 3.2, 3.3, and 3.3 nm for MAC 6, MAC12, and AC12, respectively. All the *d*-spacings are smaller than the corresponding fully extended molecular lengths, indicating possibly a tilted layered structure. This is consistent with the reported phase structure of similar LCs.[35] Thermal PLM experiment confirmed the LC phase structure, and Figure 4 shows the PLM images of MAC6, MAC12, and AC12 at 70, 80, and 76 °C, respectively (LC phase region). These LC phases are also subject to electric field switching. EO investigations were carried out in transparent sandwich type capacitor cells consisting of two indium−tin oxide (ITO)-coated glass plates (thickness 5 μm, Instec Inc.). Dramatic texture change was observed when applying rectangular electric field, as shown in Figure 4. The spherulitic domain with orthogonal extinction brushes could be observed using PLM. The extinction brushes are about 40° away from the directions of the crossed polarizers under electric field and can rotate clockwise or anticlockwise with reversing the polarity of the electric field. After switching off the voltage, the birefringence of texture dramatically decreased, and the directions of extinction brushes relaxed to the same position of the crossed polarizers. This reveals a typical tristable switching process, confirming the AF switching.[43] To measure the spontaneous polarization (Ps) of MAC12, a triangular wave was applied with a peak-to-peak voltage of 120 V and a frequency of 5 Hz. Two current peaks can be clearly identified within half period of the triangular wave as shown in Figure 5, clearly indicating the AF behavior and Ps was measured to be ~200 nC cm^{-2}. Note that MAC12 is prone to polymerize under the ac electric field; hence, all the data were measured using freshly prepared LC cells, and the measurement time was limited to be <5 min. Table 1 summarizes the phase transition temperatures and transition enthalpy values of the monomers.

Synthesis and Phase Structure of Side-Chain BCLC Polymers. Both FRP and ATRP were successfully carried out to synthesize the BCLC polymers. Since the monomers have

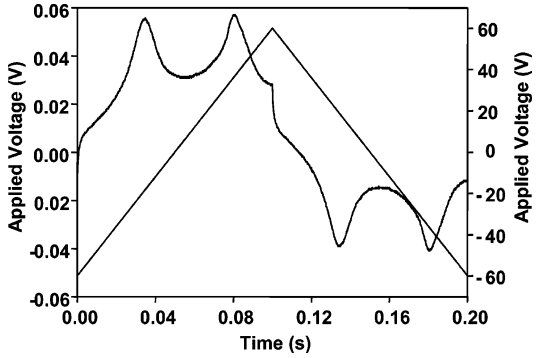

Figure 5. Switching current response of 3′-[4-(4-*n*-dodecyloxybenzoyloxy)benzoyloxy]-4-(12-methacryloyloxydodecyloxy)benzoyloxybiphenyl (MAC12) (T = 78 °C, 60 V, 5 Hz, 5 μm indium−tin oxide (ITO)-coated cell, Instec Inc.). The occurrence of two peaks in each half period of the applied triangular wave is an indication of an antiferroelectric switching process.

Table 1. Phase Transition Temperatures (t/°C) and Transition Enthalpy (δh/kJ mol^{-1}, Values in Brackets) of the Side-Chain Liquid Crystalline Monomers, 3′-[4-(4-*n*-Dodecyloxybenzoyloxy)benzoyloxy]-4-(12-acryloyloxydodecyloxy)benzoyloxybiphenyl (AC12), 3′-[4-(4-*n*-Dodecyloxybenzoyloxy)benzoyloxy]-4-(6-methacryloyloxyhexyloxy)benzoyloxybiphenyl (MAC6), and 3′-[4-(4-*n*-Dodecyloxybenzoyloxy)benzoyloxy]-4-(12-methacryloyloxydodecyloxy)benzoyloxybiphenyl (MAC12)[a]

compound	phase transition (°C [kJ/mol])
AC12	Cr 76 [34.3] $SmCP_A$ 87 [10.4] Iso
MAC6	Cr 77 [45.0] ($SmCP_A$ 65 [16.7])[b] Iso
MAC12	Cr 74 [19.9] $SmCP_A$ 82 [17.2] Iso

[a] Determined by DSC (second heating scan, 10 °C min^{-1}). Abbreviations: Cr = crystalline state, $SmCP_A$ = AF switching polar titled lamellar liquid crystalline mesophase, Iso = isotropic liquid state. [b] From first cooling scan.

poor solubility in methanol, normal precipitation process is not sufficient to remove unreacted monomers. Further purification was achieved by using the column chromatography technique. Polymer chemical structures were confirmed by ^{1}H NMR spectroscopy and GPC. As an example, Figures 1b shows the ^{1}H NMR spectra of PMAC12. The characteristic resonance of the vinyl group at 6.09 and 5.53 ppm in MAC12 completely disappeared after polymerization. Before further characterization was performed, the polymer was dried in vacuum over P_2O_5 at 70 °C for 24 h. Polymer molecular weight (MW) and polydispersity were measured by GPC using THF as the eluent. TGA (at a heating rate of 20 °C/min in dry nitrogen) showed that all the polymers had 1% weight loss above 330 °C. Table 2 summarizes the properties of the side-chain LCPs.

Figure 6 shows DSC thermograms of PMAC6, PMAC12, and PAC12. All the polymers have one sharp phase transition peak

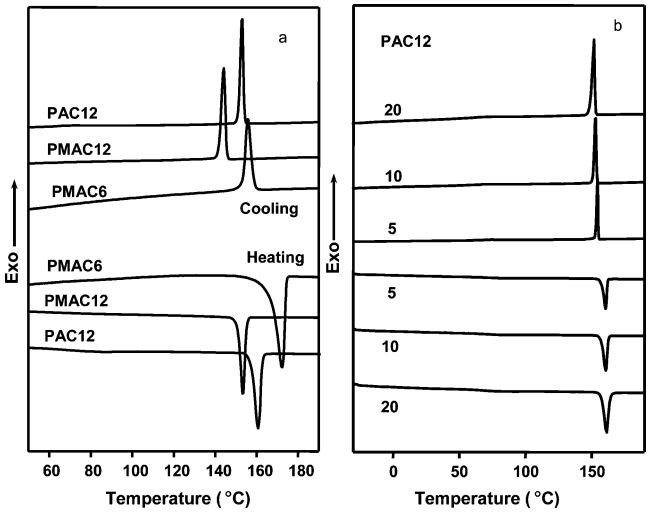

Figure 6. (a) Differential scanning calorimetry thermograms of poly{(3′-[4-(4-*n*-dodecyloxybenzoyloxy)benzoyloxy]-4-(12-acryloyloxydodecyloxy)benzoyloxybiphenyl} (PAC12), poly{3′-[4-(4-*n*-dodecyloxybenzoyloxy)benzoyloxy]-4-(6-methacryloyloxyhexyloxy)benzoyloxybiphenyl} (PMAC6), and poly{3′-[4-(4-*n*-dodecyloxybenzoyloxy)benzoyloxy]-4-(12-methacryloyloxydodecyloxy)benzoyloxybiphenyl} (PMAC12), using a 10 °C/min cooling/heating rate. (b) Differential scanning calorimetry thermograms of PAC12 with different heating and cooling rates (°C/min).

in heating and cooling experiments. A weak glass transition could be detected at 60−70 °C. The first-order phase transition is heating/cooling rate independent as shown in Figure 6b, suggesting an LC transition. Thermo-PLM was used to study the LC behavior, and Figure 7 shows the textures of the three polymers. In PAC12 and PMAC12, threaded/Schlieren textures could be detected using PLM when cooling the samples from the isotropic phase at a rate of 1 °C/min. In PMAC6, threaded/Schlieren texture can also be seen in small birefringent domains. Compared to the monomer textures, domain sizes in BCLC polymers are much smaller due to the high viscosity of the polymeric materials.

Two-dimensional (2D) WAXD and SAXS experiments were carried out to study the polymer mesophase structure. Specimens were obtained by shearing the sample (shear geometry is shown in Scheme 4) in the mesophase temperature. The fibers/films were annealed at the same temperature for several hours and then quenched to room temperature. Figure 8 shows the WAXD pattern of the PAC12 sheared film obtained at room temperature with the X-rays perpendicular to the shear direction. Six pairs of sharp diffraction arcs in the low-angle region can be clearly seen on the equator, while in the wide-angle region four diffused arcs can be seen in the quadrants. The first-order diffraction peak is very close to the beam stop, possessing a *d*-spacing of

Table 2. Synthesis and Thermal Properties of Poly{(3′-[4-(4-*n*-dodecyloxybenzoyloxy)benzoyloxy]-4-(12′-acryloyloxydodecyloxy)benzoyloxybiphenyl} (PAC12), Poly{3′-[4-(4-*n*-dodecyloxybenzoyloxy)benzoyloxy]-4-(6-methacryloyloxyhexyloxy)benzoyloxybiphenyl} (PMAC6), and Poly{3′-[4-(4-*n*-dodecyloxybenzoyloxy)benzoyloxy]-4-(12-methacryloyloxydodecyloxy)benzoyloxybiphenyl} (PMAC12)

polymer	initiator/solvent/temp[a]	yield (%)	$M_n \times 10^{-4}$ [b]	M_w/M_n[b]	T_g[c] (°C)	T_i[c] (°C)	T_d[d] (°C)
PAC12	AIBN/benzene/60 °C	65	3.7	1.2	67	161	341
PMAC6	AIBN/benzene/60 °C	75	18	1.3	73	172	346
PMAC12	AIBN/benzene/60 °C	72	22	1.4	75	153	354
PMAC12	EBP/CuBr/PMDETA/chlorobenzene/60 °C	77	4.0	1.2	74	153	350

[a] [Monomer]:[AIBN] = 300:1 (molar ratio), time = 24 h, where AIBN = 2,2′-azobis(isobutyronitrile); [monomer]:[EBP]:[CuBr]:[PMDETA] = 40:1:1:1, time = 24 h, where EBP = ethyl 2-bromopropionate, PMDETA = *N*,*N*,*N*′,*N*′,*N*″-pentamethyldiethylenetriamine. [b] Number-average molecular weight (M_n) and polydispersity (M_w/M_n, M_w = weight-average molecular weight), determined by gel permeation chromatography, using tetrahydrofuran as an eluent at 35 °C, polystyrene as standards. [c] Glass transition temperature (T_g) and isotropic temperature (T_i), determined by differential scanning calorimetry (10 °C/min, second heating). [d] Decomposition temperature (T_d) at which 5% weight loss of the sample was reached under N_2, determined by thermogravimetric analyses (10 °C/min).

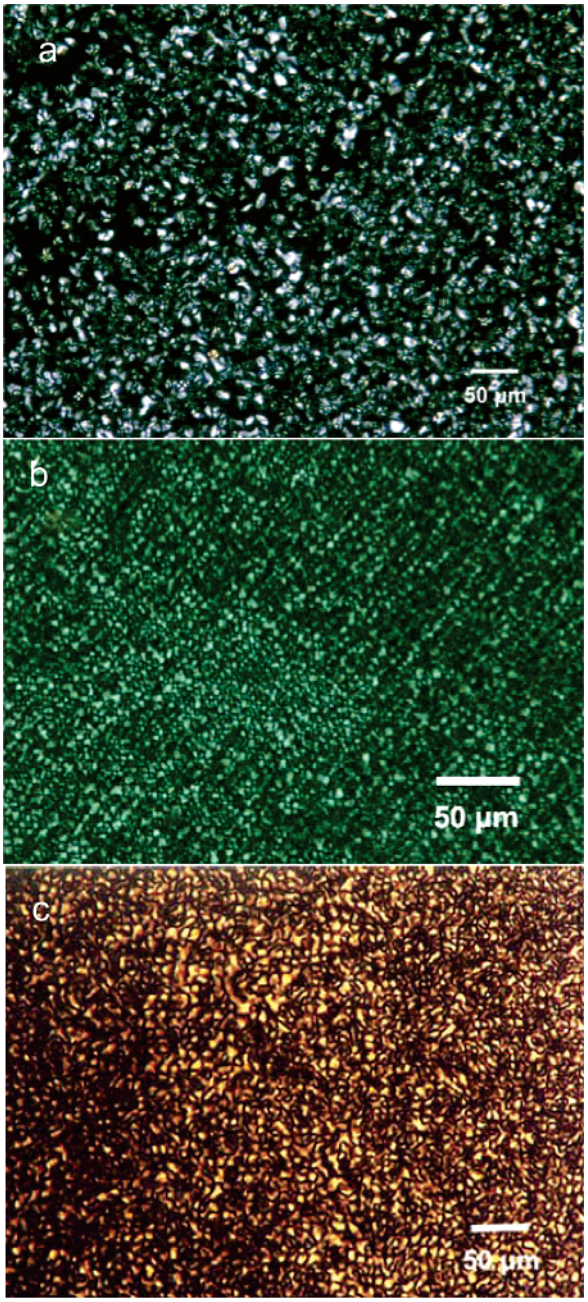

Figure 7. Thread textures of poly{(3′-[4-(4-*n*-dodecyloxybenzoyloxy)-benzoyloxy]-4-(12-acryloyloxydodecyloxy)benzoyloxybiphenyl) (PAC12) at 150 °C (a), poly{3′-[4-(4-*n*-dodecyloxybenzoyloxy)benzoyloxy]-4-(6-methacryloyloxyhexyloxy)benzoyloxybiphenyl} (PMAC6) at 155 °C (b), and poly{3′-[4-(4-*n*-dodecyloxybenzoyloxy)benzoyloxy]-4-(12-methacryloyloxydodecyloxy)benzoyloxybiphenyl} (PMAC12) at 145 °C (c).

8.17 nm (*l*), which is much larger than the calculated mesogen length in the extended conformation (5.6 nm, *L*). In order to confirm this diffraction peak, SAXS was conducted with a sample-to-detector distance of ~200 cm and the X-rays perpendicular to the shear direction. Figure 8b shows the results, and two pairs of diffraction arcs can be seen on the equator, the scattering vectors of which are in coincidence with the first and the second diffractions in the low-angle region of the WAXD pattern, indicating that all the six pairs WAXD arcs in Figure 8a are from the LC phase diffraction. Figure 8c shows the 2θ integration of Figure 8a along the equator direction. Careful analysis shows that the scattering vector ratio of the diffractions in the WAXD followed 1:2:3:4:5:6, suggesting a long-range ordered smectic structure with a layer spacing of

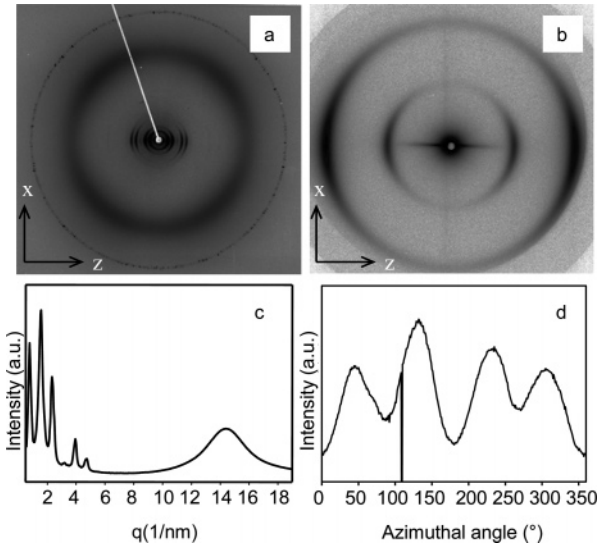

Figure 8. Two-dimensional wide-angle X-ray diffraction pattern of poly{(3′-[4-(4-*n*-dodecyloxybenzoyloxy)benzoyloxy]-4-(12-acryloyloxydodecyloxy)benzoyloxybiphenyl} (PAC12) obtained with the X-ray beam perpendicular to the shear direction (a), two-dimensional small-angle X-ray scattering pattern of sheared sample (b), 2θ integration of (a) along equator (c), and azimuthal scan of wide-angle amorphous halo (d).

~8.17 nm (*l*). Since the first-order diffraction possesses much larger *d*-spacing compared to the extended conformation of the mesogen, a bilayered structure is proposed. Observation of the bilayer structure in side-chain banana LCP is interesting, and we shall return to this issue in the following section. *l* is also smaller than 2*L*, suggesting a tilted smectic phase structure. This can be confirmed by azimuthal integration of the wide-angle diffraction arc, as shown in Figure 8d. These diffuse arcs are symmetrically placed about the meridian and form pairs of straight lines at an angle of 43° from meridian with respect to the layer normal. Therefore, smectic C nature of the LC phase can be confirmed.

PMAC6 and PMAC12 showed similar 2-D WAXD and SAXS patterns. Figure 9a shows the 2D WAXD pattern of PMAC6 with the X-rays perpendicular to the shear direction. Up to 7 orders of diffraction can be observed on the equator in the low-angle region of the diffraction pattern as shown in Figure 9c (2θ integration along the equator), and the near-beam stop diffraction was also confirmed by SAXS along the *yz* plane as depicted in Figure 9b. The two pairs of SAXS peaks correspond to the first- and second-order diffractions observed in the WAXD pattern. Bilayer smectic structure therefore was also formed in PMAC6. (PMAC12 showed a similar diffraction pattern.) Azimuthal integration of the wide-angle region (Figure 9d) again shows four peaks, indicating a 41° tilt of the banana mesogen from the smectic layer normal.

EO investigations were also carried out in similar LC cells as previously discussed. Lower MW PMAC12 (M_n = 40 000 g/mol) and PAC12 (M_n = 37 000 g/mol) were synthesized using ATRP and FRP methods. LC cells filled with both low M_w PMAC12 and PAC12 were prepared. Although LC texture change upon application of electric fields can be observed using PLM, EO switching is relatively weak. The repolarization current of PAC12 in response to an applied triangular-wave field shows two small humps per half wave function (Figure 10), indicating perhaps an AF switching behavior. The low intensity of the switching humps indicates that, due to the high viscosity of the polymer samples, not all the molecular dipoles were switched during the EO measurement.

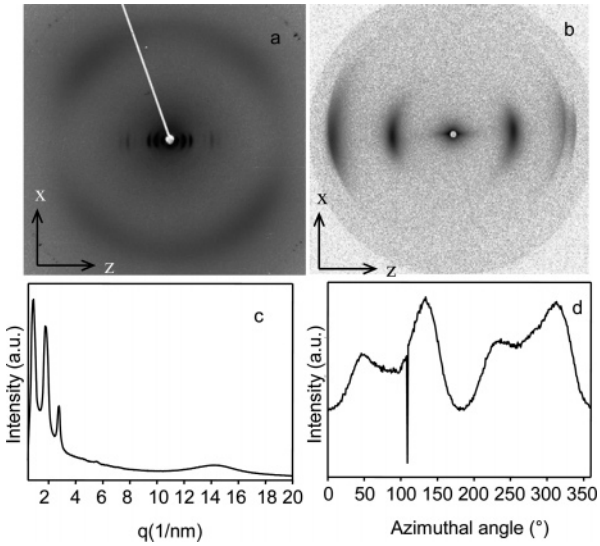

Figure 9. Two-dimensional wide-angle X-ray diffraction pattern patterns of poly{3′-[4-(4-*n*-dodecyloxybenzoyloxy)benzoyloxy]-4-(6-methacryloyloxyhexyloxy)benzoyloxybiphenyl} (PMAC6) obtained with the X-ray beam perpendicular to the shear direction (a), two-dimensional small-angle X-ray scattering pattern of sheared sample (b), 2θ integration of (a) along equator (c), and azimuthal scan of wide angle amorphous halo (d).

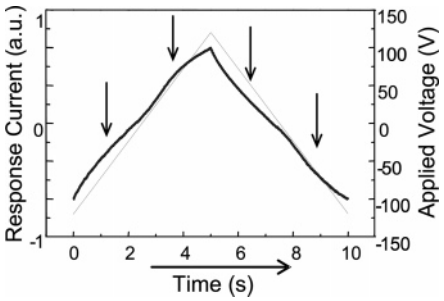

Figure 10. Switching current response of poly{(3′-[4-(4-*n*-dodecyloxybenzoyloxy)benzoyloxy]-4-(12-acryloyloxydodecyloxy)benzoyloxybiphenyl} (PAC12) (T = 152 °C, 120 V, 0.1 Hz, 5 μm ITO-coated cell, Instec). The occurrence of two humps in each half period on applying triangular wave voltage is an indication of an antiferroelectric switching process.

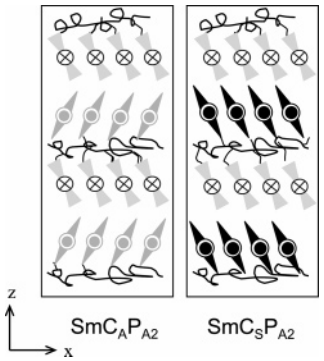

Figure 11. Schematic representation of the bilayer SmCP$_{A2}$ (smectic C denotes the LC molecules are tilted with respect to the layer normal, P indicates the layers are polar, A indicates antiferroelectric behavior, and 2 represents the bilayered structure) phase of the side-chain bent-core liquid crystalline polymers.

Figures 8 and 9 also showed that, upon shearing, smectic layers were parallel to the shear direction, while banana mesogens are tilted ~43° from the layer normal. Figure 11 shows the schematic representation of the LC phase structure. Figure 9a,d also shows that the second and fourth quadrant diffuse diffractions in the wide-angle region are much stronger than the first and third quadrant diffractions, suggesting that synclinic tilting might exist in the system.[44] Note that we did not observe similar asymmetric diffractions in PAC12, indicating that both synclinic and anticlinic might occur in these side chain systems. Accordingly, both SmC$_A$P$_{A2}$ and SmC$_S$P$_{A2}$ (2 denotes bilayer) were used in the schematic representation in Figure 11. One intriguing observation is the bilayer smectic structure. Bilayer structure is easy to form in small molecules with a strong electric dipole group at one of their ends or in polymeric systems where mesogenic units are attached to the backbone by one of their ends.[45] In BCLCs, the AF bilayer structure can be resolved using resonant X-ray diffraction. Bilayer structures observed using conventional XRD have also been reported, which was attributed to the triclinic tilting, resulting in the deviation of the molecular mass center point from the layer central lines. Thus, SmCG is normally assigned to those bilayer BCLC structures observed using conventional XRD experiment. In our system, since the monomers did not show the bilayer feature, we speculate the observation of the bilayer structure in the LCP system is due to polymer backbones sequestering every two layers of the smectic LCs, as shown in Figure 11. Electron density fluctuation with a wavelength that is double the layer thickness was thus formed, leading to a bilayer structure.

Comparing these three LCP samples, we noticed that similar LC structures were formed in LCP with different polymer backbones (PAC12 and PMAC12) as well as different spacer lengths (PMAC6 and PMAC12). This can be attributed to that the bent-shaped nature and relatively large size of BCLC mesogens dictate more packing space than the conventional calamitic mesogens. The volume fraction of the side chains is thus high, leading to a more significant influence of the side chain on the LCP behavior. Detailed experimental work is ongoing to further tailor the chemical structures (different backbones, copolymers, etc.) in order to fine-tune the LC behavior of the BCLC systems.

Conclusions

In summary, LC poly(meth)acrylates with end-on BCLC mesogens have been synthesized using FRP and ATRP methods. The resulting polymers exhibit thermotropic LC behavior. Phase structure and LC properties of both monomers and polymers were investigated. SmCP phases were identified in all the BCLC monomers. AF switching was also confirmed using EO measurement. For all the side-chain LCPs investigated, a first-order transition was found in DSC experiments. Using WAXD and SAXS techniques, smectic layer structure could be identified with a layer *d*-spacing around 7−8 nm, which is much larger than the calculated mesogen length. A bilayer SmCP$_{A2}$ phase was thus proposed. The tilting angle of the bent-core mesogen is ~41°−43°. Because of the high viscosity of the polymers, only low-M_w LCP showed measurable EO switching. Detailed investigations on the bilayer structure and how to tune the BCLC behavior via tailoring the chemical structure are underway.

Acknowledgment. This work was supported by National Natural Science Foundation of China (Grant 20504002), the National Science Foundation (NSF CAREER award, DMR-0239415), ACS-PRF, 3M, and DuPont. X.F.C. thanks the support from the Doctoral Program of the Higher Education Institution of Ministry of Education (20030001061). Synchrotron experiments were conducted at beamline X27C, NSLS in Brookhaven National Laboratory, supported by DOE.

Supporting Information Available: Synthesis and characterization of intermediates and precursors of those monomers. This

material is available free of charge via the Internet at http://pubs.acs.org.

References and Notes

(1) *Chirality in Liquid Crystals*; Kitzerow, H.-S., Bahr, C., Eds.; Springer: Berlin, 2001.
(2) Niori, T.; Sekine, T.; Watanabe, J.; Furukawa, T.; Takezoe, H. *J. Mater. Chem.* **1996**, *6*, 1231−1233.
(3) Link, D. R.; Natale, G.; Shao, R.; Maclennan, J. E.; Clark, N. A.; Korblova, E.; Walba, D. M. *Science* **1997**, *278*, 1924−1927.
(4) Heppke, G.; Moro, D. *Science* **1998**, *279*, 1872−1873.
(5) Coleman, D. A.; Fernsler, J.; Chattham, N.; Nakata, M.; Takanishi, Y.; Korblova, E.; Link, D. R.; Shao, R. F.; Jang, W. G.; Maclennan, J. E.; Mondainn-Monval, O.; Boyer, C.; Weissflog, W.; Pelzl, G.; Chien, L. C.; Zasadzinski, J.; Watanabe, J.; Walba, D. M.; Takezoe, H.; Clark, N. A. *Science* **2003**, *301*, 1204−1211.
(6) Pelzl, G.; Diele, S.; Weissflog, W. *Adv. Mater.* **1999**, *11*, 707−724.
(7) Tschierske, C.; Dantlgraber, G. *Pramana* **2003**, *61*, 455−481.
(8) Ros, M. B.; Serrano, J. L.; de la Fuente, M. R.; Folcia, C. L. *J. Mater. Chem.* **2005**, *15*, 5093−5098.
(9) Takezoe, H.; Takanishi, Y. *Jpn. J. Appl. Phys.* **2006**, *45*, 597−625.
(10) Reddy, R. A.; Tschierske, C. *J. Mater. Chem.* **2006**, *16*, 907−961.
(11) Bedel, J. P.; Rouillon, J. C.; Marcerou, J. P.; Nguyen, H. T.; Achard, M. F. *Phys. Rev. E* **2004**, *69*, 061702−9.
(12) Murthy, H. N. S.; Sadashiva, B. K. *Liq. Cryst.* **2004**, *31*, 567−578.
(13) Reddy, R. A.; Sadashiva, B. K. *J. Mater. Chem.* **2004**, *14*, 310−319.
(14) Sadashiva, B. K.; Reddy, R. A.; Pratibha, R.; Madhusudana, N. V. *J. Mater. Chem.* **2002**, *12*, 943−950.
(15) Bedel, J. P.; Rouillon, J. C.; Marcerou, J. P.; Laguerre, M.; Nguyen, H. T.; Achard, M. F. *Liq. Cryst.* **2001**, *28*, 1285−1292.
(16) Keum, C. D.; Kanazawa, A.; Ikeda, T. *Adv. Mater.* **2001**, *13*, 321−323.
(17) Lee, C. K.; Kwon, S. S.; Shin, S. T.; Choi, E. J.; Lee, S.; Chien, L. C. *Liq. Cryst.* **2002**, *29*, 1007−1013.
(18) Fodor-Csorba, K.; Vajda, A.; Galli, G.; Jakli, A.; Demus, D.; Holly, S.; Gacs-Baitz, E. *Macromol. Chem. Phys.* **2002**, *203*, 1556−1563.
(19) Sentman, A. C.; Gin, D. L. *Angew. Chem., Int. Ed.* **2003**, *42*, 1815−1819.
(20) Kwon, S. S.; Kim, T. S.; Lee, C. K.; Shin, S. T.; Oh, L. T.; Choi, E. J.; Kim, S. Y.; Chien, L. C. *Bull. Korean Chem. Soc.* **2003**, *24*, 274−278.
(21) Barbera, J.; Gimeno, N.; Monreal, L.; Pinol, R.; Ros, M. B.; Serrano, J. L. *J. Am. Chem. Soc.* **2004**, *126*, 7190−7191.
(22) Fodor-Csorba, K.; Jakli, A.; Galli, G. *Macromol. Symp.* **2004**, *218*, 81−88.
(23) Fodor-Csorba, K.; Vajda, A.; Jakli, A.; Slugovc, C.; Trimmel, G.; Demus, D.; Gacs-Baitz, E.; Holly, S.; Galli, G. *J. Mater. Chem.* **2004**, *14*, 2499−2506.
(24) Lee, C. K.; Kwon, S. S.; Kim, T. S.; Shin, S. T.; Chow, H.; Choi, E. J.; Kim, S. Y.; Zin, W. C.; Kim, D. C.; Chien, L. C. *Bull. Korean Chem. Soc.* **2004**, *25*, 1171−1176.
(25) Novotna, V.; Hamplova, V.; Kaspar, M.; Glogarova, M.; Pociecha, D. *Liq. Cryst.* **2005**, *32*, 1115−1123.
(26) Achten, R.; Koudijs, A.; Giesbers, M.; Marcelis, A. T. M.; Sudholter, E. J. R. *Liq. Cryst.* **2005**, *32*, 277−285.
(27) Kozmik, V.; Kovarova, A.; Kuchar, M.; Svoboda, J.; Novotna, V.; Glogarova, M.; Kroupa, J. *Liq. Cryst.* **2006**, *33*, 41−56.
(28) Galli, G.; Demel, S.; Slugovc, C.; Stelzer, F.; Weissflog, W.; Diele, S.; Fodor-Csorba, K. *Mol. Cryst. Liq. Cryst.* **2005**, *439*, 1909−1919.
(29) Gallastegui, J. A.; Folcia, C. L.; Etxebarria, J.; Ortega, J.; Gimeno, N.; Ros, M. B. *J. Appl. Phys.* **2005**, *98*, 083501−4.
(30) Demel, S.; Slugovc, C. F. S.; Fodor-Csorba, K.; Galli, G. *Macromol. Rapid Commun.* **2003**, *24*, 636−641.
(31) Choi, E. J.; Ahn, J. C.; Chien, L. C.; Lec, C. K.; Zin, W. C.; Kim, D. C.; Shin, S. T. *Macromolecules* **2004**, *37*, 71−78.
(32) Chen, X. F.; Tenneti, K. K.; Li, C. Y.; Bai, Y. W.; Zhou, R.; Wan, X. H.; Fan, X. H.; Zhou, Q. F. *Macromolecules* **2006**, *39*, 517−527.
(33) Keith, C.; Reddy, R. A.; Tschierske, C. *Chem. Commun.* **2005**, 871−873.
(34) Dantlgraber, G.; Eremin, A.; Diele, S.; Hauser, A.; Kresse, H.; Pelzl, G.; Tschierske, C. *Angew. Chem., Int. Ed.* **2002**, *41*, 2408−2412.
(35) Keith, C.; Reddy, R. A.; Hauser, A.; Baumeister, U.; Tschierske, C. *J. Am. Chem. Soc.* **2006**, *128*, 3051−3066.
(36) Jakli, A.; Lischka, C.; Weissflog, W.; Pelzl, G. *Liq. Cryst.* **2000**, *27*, 715−719.
(37) Mieczkowski, J.; Gomola, K.; Koseska, J.; Pociecha, D.; Szydlowska, J.; Gorecka, E. *J. Mater. Chem.* **2003**, *13*, 2132−2137.
(38) Schroder, M. W.; Diele, S.; Pelzl, G.; Dunemann, U.; Kresse, H.; Weissflog, W. *J. Mater. Chem.* **2003**, *13*, 1877−1882.
(39) Achten, R.; Cuypers, R.; Giesbers, M.; Koudijs, A.; Marcelis, A.; Sudholter, E. *Liq. Cryst.* **2004**, *31*, 1167−1174.
(40) Novotna, V.; Kaspar, M.; Hamplova, V.; Glogarova, M.; Lejcek, L.; Kroupa, J.; Pociecha, D. *J. Mater. Chem.* **2006**, *16*, 2031−2038.
(41) Shen, D.; Diele, S.; Wirt, I.; Tschierske, C. *Chem. Commun.* **1998**, 2573−2574.
(42) Shen, D.; Pegenau, A.; Diele, S.; Wirth, I.; Tschierske, C. *J. Am. Chem. Soc.* **2000**, *122*, 1593−1601.
(43) Reddy, R. A.; Sadashiva, B. K. *Liq. Cryst.* **2003**, *30*, 1031−1050.
(44) Keith, C.; Reddy, R. A.; Baumeister, U.; Tschierske, C. *J. Am. Chem. Soc.* **2004**, *126*, 14312−14313.
(45) Davidson, P. *Prog. Polym. Sci.* **1996**, *21*, 893−950.

MA061949U